


RESEARCH ARTICLE OPEN ACCESS

Cytotoxic and Antileishmanial Potential of *Pilocarpus microphyllus* Essential Oil: In Vitro and In Silico Study

Juniel Cruz Silva¹ | Maria Gabriela Araújo Mendes² | Paulo Sérgio de Araujo Sousa¹ | Alyne Rodrigues de Araújo Nobre¹ | Michel Muálem de Moraes Alves³ | Fernando Aécio de Amorim Carvalho³ | Tatiane Caroline Daboit² | José de Sousa Lima Neto⁴ | Ygor Victor Ferreira Pinheiro¹ | Ytallo da Costa Sousa¹ | Edymilaís da Silva Sousa⁵ | José Delano Barreto Marinho Filho⁶ | Ana Jérsia Araújo⁶ | Francisco Artur Silva Filho⁷ | Sidney Gonçalo de Lima² | Leiz Maria Costa Vêras¹ 

¹Biodiversity and Biotechnology Research Center, BIOTEC, Federal University of Delta do Parnaíba (UFDPAR), Parnaíba, Brazil | ²Advanced Study Group in Medical Mycology, GEAMICOL, Federal University of Delta do Parnaíba (UFDPAR), Parnaíba, Brazil | ³Laboratory of Antileishmania Activity, LAA, Medicinal Plants Research Center, NPPM, Federal University of Piauí, UFPI, Teresina, Brazil | ⁴Pharmacy Department, Health Sciences Center, Federal University of Piauí (UFPI), Teresina, Brazil | ⁵Organic Geochemistry Laboratory, Natural Sciences Center, Federal University of Piauí (UFPI), Teresina, Brazil | ⁶Delta Cell Culture Laboratory, LCCDelta, Federal University of Delta do Parnaíba (UFDPAR), Parnaíba, Brazil | ⁷State University of Piauí, Parnaíba, Brazil

Correspondence: Leiz Maria Costa Vêras (leiz@ufdpar.edu.br)

Received: 30 June 2025 | **Revised:** 23 December 2025 | **Accepted:** 29 December 2025

Keywords: γ -cadinene | cytotoxicity | molecular docking | *Pilocarpus microphyllus* | *trans*-caryophyllene

ABSTRACT

The essential oil of *Pilocarpus microphyllus* (jaborandi) (EOJ), a species traditionally recognized for its alkaloid-based pharmacological properties, remains poorly investigated despite its richness in bioactive terpenes. In this study, the chemical profile of EOJ obtained from fresh and dried leaves was determined by gas chromatography-mass spectrometry, revealing 24 constituents, predominantly γ -cadinene (23.6%) and *trans*-caryophyllene (22.9%). Antifungal activity was observed against *Cryptococcus neoformans* (minimum inhibitory concentration: 149–2395 $\mu\text{g/mL}$), while antileishmanial potential was confirmed against *Leishmania amazonensis* promastigotes (half-maximal inhibitory concentration [IC_{50}]: 22.8–25.2 $\mu\text{g/mL}$). EOJ also exhibited cytotoxic effects on HCT-116 and PC-3 cell lines (IC_{50} : 27.8–29.2 $\mu\text{g/mL}$). In silico studies revealed strong binding affinities with therapeutic targets: γ -cadinene to Nectin-4 ($\Delta G = -7.3$ kcal/mol) and *trans*-caryophyllene to lanosterol 14 α -demethylase ($\Delta G = -5.7$ kcal/mol). Absorption, distribution, metabolism, excretion, and toxicity predictions indicated favorable oral absorption and low genotoxicity. Altogether, EOJ demonstrates multitarget bioactivity, and its major constituents represent promising leads for antifungal, antileishmanial, and anticancer drug development.

1 | Introduction

Pilocarpus microphyllus Stapf (Rutaceae), commonly known as jaborandi, is an endemic species of the Amazon and northeastern Brazil and has traditionally been exploited for the production of pilocarpine, an alkaloid widely used in the treatment of glaucoma, xerostomia, and xerophthalmia [1, 2]. More recently, other alkaloids such as epiisopiloturine have been reported to

display antiparasitic activity against *Schistosoma mansoni* and cardioprotective effects, further reinforcing the pharmacological potential of the species [3, 4].

Despite the prominence of its alkaloids, the essential oil (EO) of *P. microphyllus* (jaborandi) (EOJ) remains poorly investigated. Essential oils have garnered attention in recent years due to their rich composition of terpenes, major secondary metabolites, with

This is an open access article under the terms of the [Creative Commons Attribution](https://creativecommons.org/licenses/by/4.0/) License, which permits use, distribution and reproduction in any medium, provided the original work is properly cited.

© 2026 The Author(s). *Chemistry & Biodiversity* published by Wiley-VHCA AG.

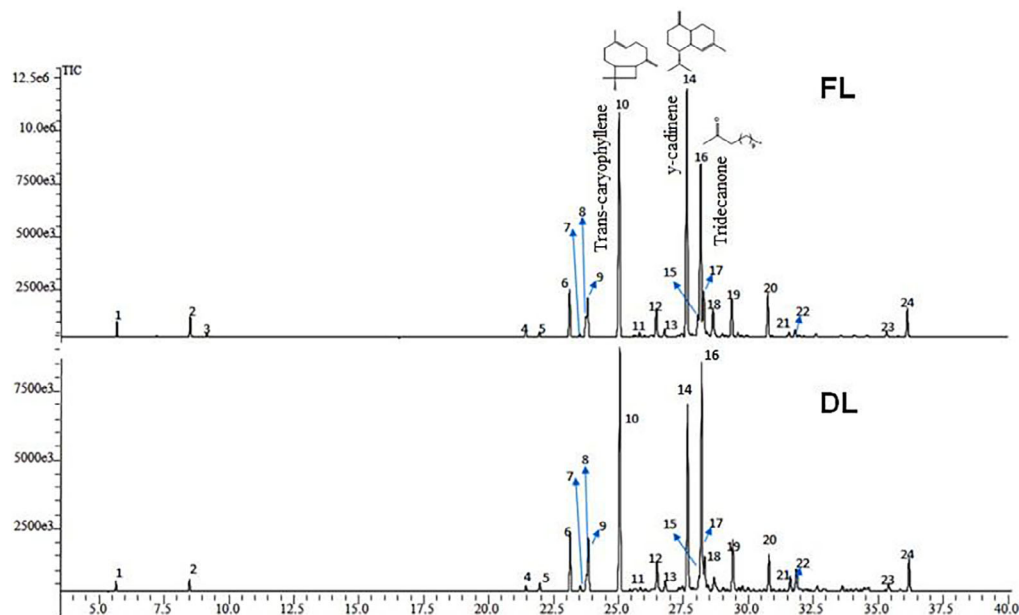


FIGURE 1 | Chromatograms show the chemical structures of the constituents of the essential oil extracted from the *P. microphyllus* (commonly known as jaborandi) leaves.

diverse bioactivities. Recent reviews confirm their antibacterial, antifungal, antioxidant, cytotoxic, and antileishmanial properties [5, 6]. Preliminary evidence suggests that the EOJ may exhibit relevant chemical and biological properties, although these remain largely unexplored, emphasizing the need for comprehensive studies to assess its therapeutic potential and pharmacological applications. In this context, the search for new bioactive molecules from the EOJ is particularly relevant in the context of pressing global health challenges, including antimicrobial resistance, which threatens the efficacy of current therapies [7]; neglected tropical diseases such as leishmaniasis, which lack safe and effective treatments due to their epidemiological and ecological complexity [8]; and cancer, the leading cause of mortality worldwide, where natural compounds continue to serve as a cornerstone for drug development [9]. Similarly, the chemical characterization and biological evaluation of *P. microphyllus* essential oil may represent a valuable strategy for the identification of new natural agents with distinct pharmacological properties.

The present study aimed to investigate the chemical composition of the essential oil obtained from fresh (FL) and dried leaves (DL) of *P. microphyllus* and to assess its antifungal, antileishmanial, and cytotoxic activities, supported by *in silico* analyses to elucidate potential molecular mechanisms of action.

2 | Results and Discussion

2.1 | Chemical Composition of the Essential Oil (Gas Chromatography Coupled With Mass Spectrometry)

The extraction of EOJ from FL and DL of *P. microphyllus* via steam distillation yielded 10.47 and 12.11 g, respectively. The mass of plant material used in each extraction was 6.400 g for FL and

4.500 g for DL. Based on these values, the mass yield (m/m) was calculated as the ratio between the mass of EOJ obtained and the mass of plant material processed. The resulting yields were 0.16% for FL and 0.27% for DL, indicating greater extraction efficiency in the dehydrated material.

Gas chromatography coupled with mass spectrometry (GC-MS) analysis allowed the identification of 24 compounds (Figure 1), including monoterpenes, sesquiterpenes, and aliphatic ketones. The major constituents were γ -cadinene (up to 23.62%), *trans*-caryophyllene (up to 22.95%), and 2-tridecanone (up to 20.92%). It was observed that the drying process led to a relative reduction of volatile compounds, particularly monoterpenes and some sesquiterpenes, which explains the compositional differences between FL-EOJ and DL-EOJ [10, 11]. Reports on the EOJ remain scarce, with only a few studies describing its volatile composition [12, 13]. However, EO from other *Pilocarpus* species, such as *Pilocarpus pennatifolius* and *Pilocarpus giganteus*, have also been reported to be rich in sesquiterpene hydrocarbons, mainly caryophyllene- and cadinene-type derivatives [14], which is consistent with the predominance observed in *P. microphyllus*.

Gas chromatography coupled with mass spectrometry (GC-MS) analysis enabled the identification of 24 compounds (Figure 1 and Table 1), including monoterpenes, sesquiterpenes, and aliphatic ketones (Table 2). The major constituents were γ -cadinene (up to 23.62%), *trans*-caryophyllene (up to 22.95%), and 2-tridecanone (up to 20.92%).

It was observed that the drying process led to a relative reduction in volatile compounds, particularly monoterpenes and some sesquiterpenes, which explains the compositional differences between FL-EOJ and DL-EOJ [10, 11, 15]. These constituents have been widely associated in the literature with antimicrobial, antioxidant, and cytotoxic activities.

TABLE 1 | Chemical composition of the essential oil of *P. microphyllus*, showing retention index (IK), Literature RI, retention time, identified compounds, and their mean relative abundance (%) with standard deviation. Relative abundances are reported as mean \pm SD from three replicate injections ($n = 3$).

Pick	Experimental IK	Literature RI	Retention time	Compound	Mean relative abundance and relative standard deviation		
1	941	932 [16]	5.67	α -Pinene	0.8	\pm	0.01
2	1010	1024 [16]	8.5	Limonene	1.45	\pm	0.02
3	1026	1037 [17]	9.15	<i>trans</i> - β -Ocimene	0.3	\pm	0.01
4	1328	1337 [18]	21.45	δ -Elemene	0.49	\pm	0.01
5	1341	1347 [16]	21.98	α -Cubebene	0.53	\pm	0.01
6	1370	1374 [16]	23.15	α -Copaene	4.25	\pm	0.01
7	1379	1388 [17]	23.54	β -Bourbonene	0.35	\pm	0.01
8	1385	1485 [17]	23.77	Germacrene D	1.7	\pm	0.04
9	1386	1389 [16, 17]	23.84	β -Elemene	3.59	\pm	0.05
10	1416	1417 [16]	25.06	<i>trans</i> -Caryophyllene	21.43	\pm	0.04
11	1436	1439 [17]	25.84	α -Guaiene	0.42	\pm	0.01
12	1448	1454 [16]	26.49	α -Humulene	2.74	\pm	0.04
13	1459	1460 [16]	26.81	Aromadendrene	0.78	\pm	0.01
14	1481	1495 [16]	27.68	γ -amorphene	23.53	\pm	0.12
15	1491	1373 [19]	28.1	Isolatedene	1.91	\pm	0.06
16	1497	1500 [16]	28.21	Tridecanone	16.15	\pm	0.06
17	1496	1500 [16]	28.32	Bicyclogermacrene	4.36	\pm	0.03
18	1505	1502 [20]	28.68	δ -Guaiene	3.21	\pm	0.01
19	1523	1538 [21]	29.41	β -Cadinene	3.61	\pm	0.1
20	1557	1561 [17]	30.8	Germacrene B	4.13	\pm	0.02
21	1583	1625 [22]	31.62	Dehydroaromadendrene	0.49	\pm	0.01
22	1589	1503 [18]	31.85	β -Guaiene	0.77	\pm	0.03
23	1680	1503 [18]	35.39	β -Guaiene	0.54	\pm	0.01
24	1700	1697 [17]	36.18	Pentadecan-2-one	2.52	\pm	0.01

TABLE 2 | Sum of the chemical classes identified in the essential oil of *P. microphyllus*. Values are derived from Table 1 mean relative abundances ($n = 3$ injections) and are presented descriptively.

Chemical class	Relative abundance (%)
Monoterpene hydrocarbons	2.25
Sesquiterpene hydrocarbons	78.93
Others (aliphatic ketones)	18.67
Total	99.85

2.2 | Antibacterial Activity

No significant antibacterial activity was observed against *Staphylococcus aureus* (ATCC 25923) or *Escherichia coli* (ATCC 25922), even at the highest concentrations tested ($>4790 \mu\text{g/mL}$). This finding corroborates previous reports on the EO of *Pilocarpus* spp., which have also shown limited antibacterial activity against both Gram-positive and Gram-negative bacteria [13, 14].

2.3 | Antifungal Activity

The antifungal properties of FL/DL-EOJ (Table 1) were similar for *Cryptococcus neoformans* strains, with minimum inhibitory concentration (MIC) values of $2395 \mu\text{g}\cdot\text{mL}^{-1}$. However, *C. neoformans* ATCC 32269 was more sensitive to FL-EOJ (MIC = $149 \mu\text{g}\cdot\text{mL}^{-1}$). According to literature guidelines, MIC values $\leq 100 \mu\text{g}\cdot\text{mL}^{-1}$ are considered strong activity, $100\text{--}500 \mu\text{g}\cdot\text{mL}^{-1}$ moderate activity, $500\text{--}1000 \mu\text{g}\cdot\text{mL}^{-1}$ weak activity, and $>1000 \mu\text{g}\cdot\text{mL}^{-1}$ inactivity [23, 24]. Based on these criteria, the EOJ showed moderate activity against *C. neoformans* ATCC 32269. The growth of *Candida krusei* ATCC 6258 and *Candida parapsilosis* ATCC 22019 was not inhibited by DL-EOJ; however, it was inhibited by FL-EOJ (MIC = $4790 \mu\text{g}\cdot\text{mL}^{-1}$) for both microorganisms [25]. They reported similar results when essential oils from *Citrus limetta*, *Citrus aurantium*, and *Citrus aurantiifolia* Swingle (Rutaceae) were tested against *Candida* spp., showing that all strains were sensitive to the respective oils. In general, fungi such as *Candida* spp. tend to be sensitive to essential oils [26], possibly due to penetration of the fungal cell wall and disruption of mitochondrial membranes, compromising fungal vitality and

TABLE 3 | Minimum inhibitory concentration (MIC) of FL-EOJ and DL-EOJ against fungal strains. MIC values were determined by broth microdilution (CLSI M27-A3) using technical triplicates ($n = 3$ wells per condition) and are reported as the lowest concentration showing no visible growth. Because MIC is a threshold/ordinal endpoint, results are presented descriptively (no inferential statistics).

Microorganism	DL	FL	Amph B
<i>Cryptococcus neoformans</i> ATCC 32269	598 $\mu\text{g/mL}$	149 $\mu\text{g/mL}$	16 $\mu\text{g/mL}$
<i>Cryptococcus neoformans</i> ATCC 24066	2395 $\mu\text{g/mL}$	2395 $\mu\text{g/mL}$	4 $\mu\text{g/mL}$
<i>Candida krusei</i> ATCC 6258	>4790 $\mu\text{g/mL}$	4790 $\mu\text{g/mL}$	1 $\mu\text{g/mL}$
<i>Candida parapsilosis</i> ATCC 22019	>4790 $\mu\text{g/mL}$	4790 $\mu\text{g/mL}$	2 $\mu\text{g/mL}$
<i>Candida albicans</i> ATCC 10231	>4790 $\mu\text{g/mL}$	>4790 $\mu\text{g/mL}$	1 $\mu\text{g/mL}$

TABLE 4 | Molecular affinity parameters of γ -cadinene, *trans*-caryophyllene, and tridecanone with 6UEZ protein.

Complex (Ligand-Protein)	$\Delta\text{G}_{\text{bind}}^{\text{[a]}}$ (kcal.mol ⁻¹)	Amino acids that interact with ligand ^[b]
γ -cadinene-6UEZ	-7.4	PHE B: 234, THR B: 315, ILE B: 377, LEU B: 310, ILE B: 488, PHE B: 139, TYR B: 145, TYR B: 131, MET B: 381, THR B: 135, LEU B: 134
<i>trans</i> -Caryophyllene-6UEZ	-8	ALA B: 311, THR B: 315, PHE B: 139, LEU B: 310, PHE B: 324, THR B: 135, ILE B: 488, LEU B: 134, ILE B: 377, TYR B: 131, MET B: 380, TYR B: 145
Tridecanone-6UEZ	-5.4	ILE B: 488, LEU B: 310, PHE B: 234, MET B: 487, LEU B: 134, MET B: 381, TYR B: 145, MET B: 380, THR B: 135, TYR B: 131, ILE B: 377, PHE B: 139

^[a]Power bond in best conformation.

^[b]Obtained with the Discovery Studio 2021 Client program.

leading to apoptosis [26–28]. However, further studies are needed to better clarify the mechanism of EOJ.

Cryptococcus neoformans is an opportunistic, encapsulated yeast responsible for cryptococcosis, a life-threatening infection that primarily affects immunocompromised individuals, such as HIV/AIDS patients and transplant recipients. It can cause severe meningoencephalitis and pneumonia, representing a major cause of morbidity and mortality worldwide, particularly in low- and middle-income countries (Table 3) [29, 30].

2.4 | Molecular Docking Studies Against Fungal Targets

The molecular docking results for the ligands with the proteins are presented in Table 4. Optimal molecular affinity parameters were obtained from the interaction between the *trans*-caryophyllene ligand with the protein 6UEZ-14a-demethylase. The affinity was observed with a binding energy equal to -8 kcal.mol⁻¹ (Table 4 and Figure 2). Interactions between the ligands and residues from active site proteins are described in Table 4.

Docking simulations with fungal enzymes confirmed favorable binding of γ -cadinene and *trans*-caryophyllene to the active sites of lanosterol 14 α -demethylase and other related proteins, supporting their role in membrane disruption and fungal growth inhibition.

2.5 | In Vitro Antileishmanial Activity

FL-EOJ and DL-EOJ inhibited the growth of promastigote forms of *L. amazonensis* after 48 h of incubation (Figure 3). Complete parasite inhibition was observed at 800 $\mu\text{g}\cdot\text{mL}^{-1}$ for both oils. The EOJ demonstrated superior antileishmanial activity compared to several essential oils from other Rutaceae and Lamiaceae species. For instance, *Lippia sidoides* and *Ocimum gratissimum* oils have been reported with IC₅₀ values of 44 and 135 $\mu\text{g}\cdot\text{mL}^{-1}$, respectively, against *L. amazonensis* promastigotes [31, 32]. These differences may be attributed to the higher proportion of sesquiterpenes such as γ -cadinene and *trans*-caryophyllene in EOJ, which possess strong lipophilicity and membrane-permeation capacity. Similar results were observed in *Zornia brasiliensis* essential oil, rich in caryophyllene derivatives, which also demonstrated IC₅₀ values below 50 $\mu\text{g}\cdot\text{mL}^{-1}$ in promastigote assays [33].

We selected the promastigote stage because it represents the extracellular form that is easier to culture under laboratory conditions and is commonly employed in preliminary screenings of natural products. Assays with intracellular amastigotes require more complex experimental models involving host macrophages, which were beyond the scope of the present study. We acknowledge this as a limitation and highlight that further investigations are necessary to confirm the activity against amastigotes, the clinically relevant stage of the parasite. *L. amazonensis* is the causative agent of cutaneous leishmaniasis in Latin America, including diffuse cutaneous leishmaniasis, a severe form often refractory to conventional therapy [34, 35].

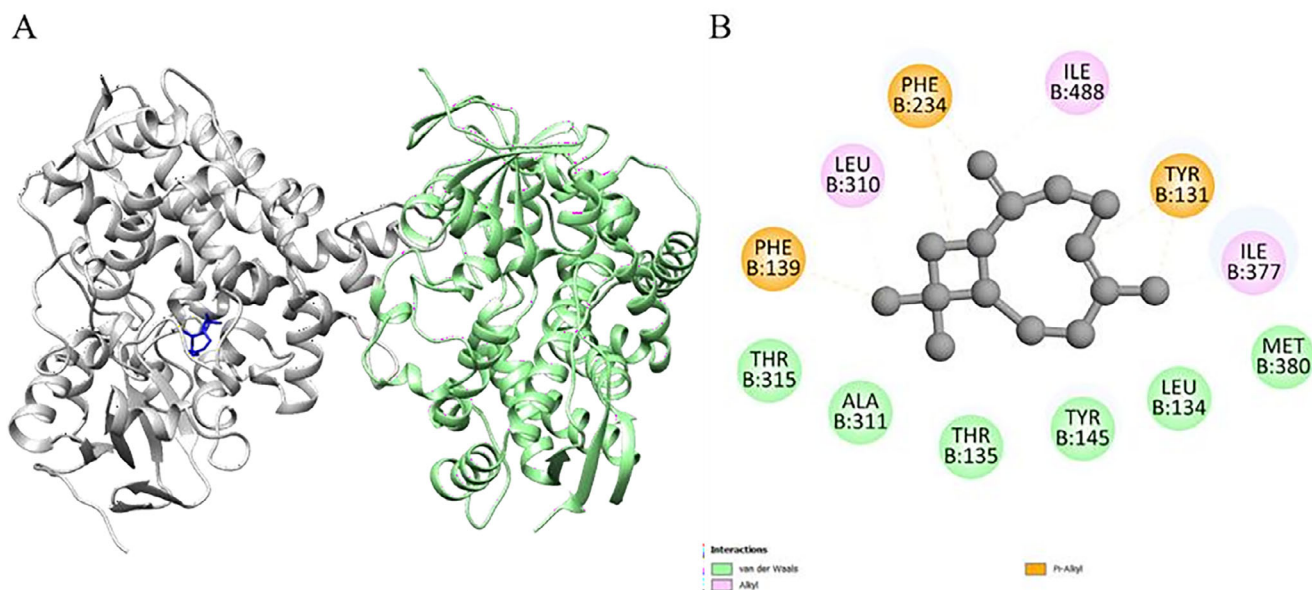


FIGURE 2 | 3D molecular docking of the protein-ligand complex with 6UEZ—Lanosterol 14 α -demethylase (Chain A color: green; Chain B color: gray) and ligand *trans*-caryophyllene (Color: blue), illustrating the active binding site (A) with the respective interactions (B) with amino acids.

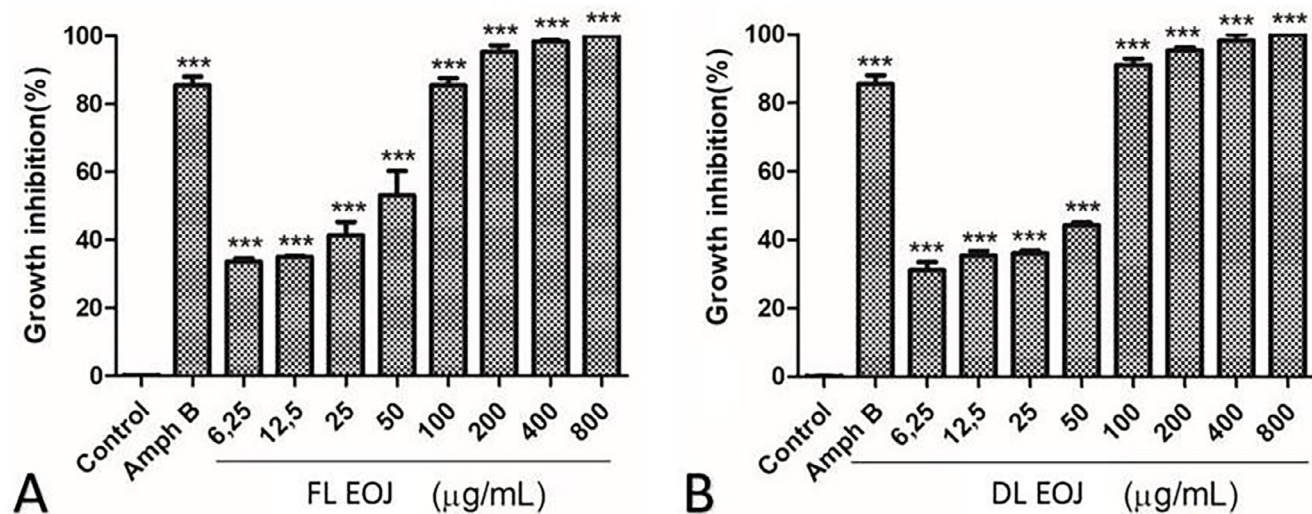


FIGURE 3 | Growth inhibition (%) of *Leishmania amazonensis* promastigotes after exposure to essential oils obtained from fresh leaves (A, FL-EOJ) and dry leaves (B, DL-EOJ) of *P. microphyllus* (6.25–800 $\mu\text{g/mL}$). Amphotericin B was used as a positive control, and vehicle (1% DMSO) as a negative control. Data are expressed as mean \pm SD from three independent experiments ($n = 3$), each performed in triplicate wells; error bars represent SD. Statistical differences versus the negative control (vehicle, 1% DMSO) were evaluated by one-way analysis of variance (ANOVA) followed by Dunnett's multiple-comparisons test. $p < 0.05$ vs negative control.

According to Raut and Karuppaiyl [6, 36], the presence of α -copaene and δ -cadinene compounds may justify their antileishmanial activity because they are lipophilic molecules. This facilitates their penetration through the parasite membrane, where they may interfere with lipid and protein metabolic pathways involved in mitochondrial membrane depolarization, ultimately leading to cellular necrosis or apoptosis. Ogungbe and Setzer, and Soto-Sánchez [37, 38] proposed that such activity can be associated with the presence of terpenoids, which are hydrocarbons with antiparasitic effects on different *Leishmania* species. Although strong hypotheses have been raised, it is not possible to determine which compound is solely responsible for

the biological activity observed, as other components present in low concentrations may also contribute [39].

2.6 | Molecular Docking Studies Against *Leishmania* Targets

In order to elucidate the possible molecular mechanisms associated with the antileishmanial activity observed in vitro in the EOJ, molecular docking simulations were conducted with two target proteins associated with the metabolism and survival of the parasite *Leishmania* spp.: the protein 1LML (leishmanolysin).

TABLE 5 | Molecular affinity parameters of γ -cadinene, *trans*-caryophyllene, and tridecanone with proteins 1LML—Leishmanolysin (*Leishmania* target).

Complex (Ligand-Protein)	$\Delta G_{\text{bind}}^{\text{[a]}}$ (kcal.mol ⁻¹)	Amino acids that interact with ligand ^[b]
γ -cadinene-1LML	-5.6	Val A: 569, Tyr A: 254, Lys A: 573, His A: 159, Leu A: 167, Gln A: 166, Gln A: 163, Thr A: 259
<i>trans</i> -Caryophyllene-1LML	-5.7	Pro A: 162, Ile A: 161, Val A: 113, Val A: 165, Lys A: 158, Val A: 157
Tridecanone-1LML	-3.9	Gly A: 567, Gln A: 566, Glu A: 376, Arg A: 171, Arg A: 260, Val A: 569, Thr A: 259, Leu A: 167, Gln A: 163, Gln A: 166

^[a] Power bond in best conformation.

^[b] Obtained with the Discovery Studio 2021 Client program.

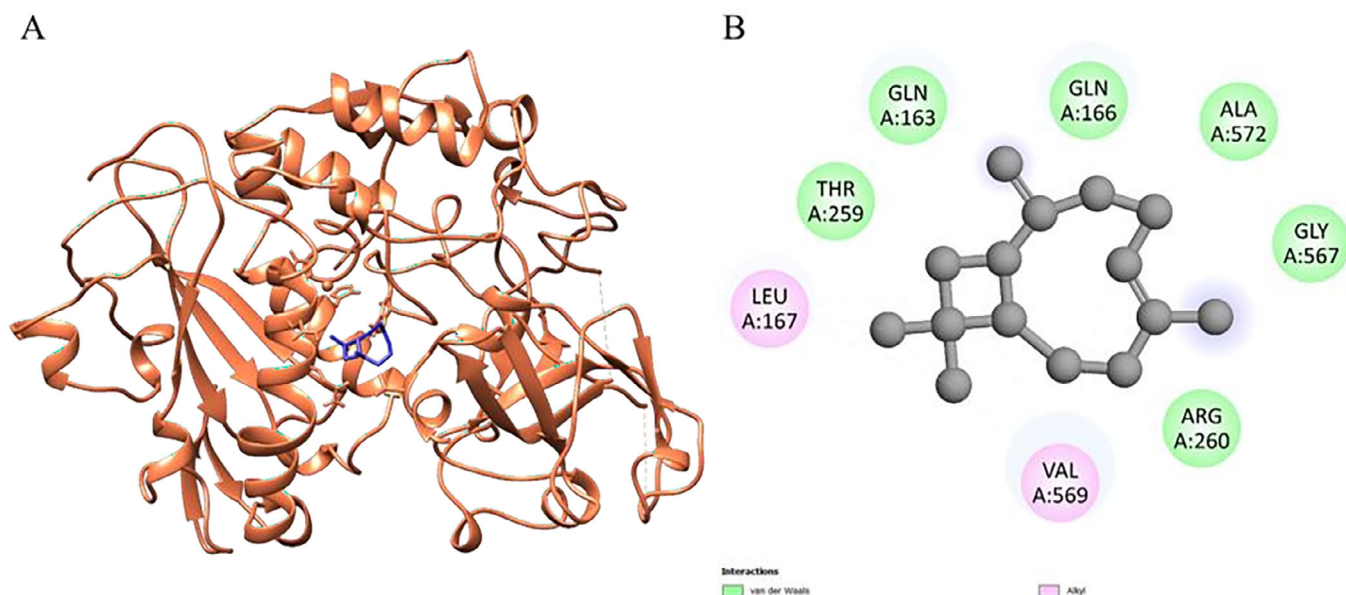


FIGURE 4 | 3D molecular docking of the ligand-protein complex with 1LML—leishmanolysin from *L. major* (chain A color: coral) and *trans*-caryophyllene (color: blue), illustrating the active binding site (A) with the respective interactions (B).

The active sites of these proteins were defined using the CASTp 3.0 server, which revealed well-defined catalytic regions, with volumes and areas suitable for the docking of the tested compounds. The results indicated relevant binding affinities between the main constituents of the essential oil and the two proteins. *trans*-Caryophyllene showed the best binding free energy with the 1LML protein, with $\Delta G_{\text{bind}} = -5.7$ kcal.mol⁻¹, interacting with hydrophobic residues such as Pro A:162, Ile A:161, Val A:113, Val A:165, and Lys A:158. Such interactions, mostly of the alkyl and van der Waals type, indicate a good fit of the ligand in the active site of the enzyme, which may impact the inhibition of critical processes of the parasite's ergosterol cycle.

Observations on the synergy between β -caryophyllene oxide and lupenone [40] support the hypothesis that mixtures can increase efficacy and selectivity. Furthermore, *Plinia cauliflora* oil, containing approximately 24% β -*cis*-caryophyllene, showed IC₅₀ in amastigotes of ~ 7 $\mu\text{g}/\text{mL}$ with high selectivity [41]. Finally, nanoemulsion application also shows promise for improving β -caryophyllene delivery and potentiating antiparasitic activity [42].

The γ -cadinene demonstrated affinity for both proteins (Table 5): $\Delta G_{\text{bind}} = -5.6$ kcal.mol⁻¹ with 1LML and -5.2 kcal.mol⁻¹. These interactions were also predominantly hydrophobic, suggesting that γ -cadinene may act on multiple molecular targets in the parasite, interfering with essential metabolic pathways. In turn, tridecanone exhibited the lowest binding affinities, with $\Delta G_{\text{bind}} = -3.9$ kcal.mol⁻¹ (1LML), indicating a less expressive role in the antileishmanial activity of the oil. The lower capacity to form significant interactions, added to the high number of rotatable bonds, may explain its poor computational performance compared to parasitic proteins.

Figure 4 presents the results obtained through molecular docking analysis between the *trans*-caryophyllene compound and the leishmanolysin from *Leishmania major* (PDB ID: 1LML), a zinc-dependent metalloprotease abundantly expressed on the surface of *Leishmania* promastigotes, which is recognized as one of the major virulence factors of the parasite. This glycoprotein plays a crucial role in parasite survival and host-parasite interactions by cleaving complement component C3b into iC3b, thereby preventing complement-mediated lysis and

TABLE 6 | Cytotoxicity (IC₅₀) of FL-EOJ and DL-EOJ in tumor cell lines. IC₅₀ values (μg/mL) were obtained by nonlinear regression of dose–Response curves and are reported with 95% confidence intervals (CI 95%). Data derived from at least three independent experiments performed in duplicate. Analyses were performed in GraphPad Prism (v6.0, San Diego, CA, USA). IC₅₀ estimates are reported descriptively; no hypothesis testing was performed to compare IC₅₀ values between samples.

Samples	HCT-116	PC-3
FL-EOJ	28.4 (26.3–30.8)	27.8 (21.6–35.8)
DL-EOJ	29.2 (27.5–31.1)	28.7 (18.0–45.7)
Doxorubicin	0.01 (0.01–0.02)	0.0016 (0.0014–0.0018)

facilitating silent entry into macrophages through complement receptor 3 (CR3) [43]. In addition, gp63 modulates host immune responses by degrading signaling molecules (such as NF-κB and MAPK), reducing macrophage activation, and impairing pro-inflammatory cytokine production [44]. It also participates in the degradation of extracellular matrix proteins, contributing to parasite dissemination within host tissues [45]. Figure 4A shows the three-dimensional representation of the protein's A chain (in coral), highlighting the positioning of *trans*-caryophyllene (in blue) inserted into the active cavity of the catalytic site, indicating good spatial complementarity between the ligand and the protein.

Figure 4B details the main physicochemical interactions established between *trans*-caryophyllene and the residues of the active cavity. Predominant van der Waals interactions were observed with residues GLN A:163, GLN A:166, ALA A:572, GLY A:567, THR A:259, and ARG A:260. These weak but numerous interactions contribute cumulatively to the stabilization of the ligand-protein complex, favoring the docking of the compound within the active site. In addition, hydrophobic alkyl interactions were established with residues VAL A:569 and LEU A:167, reinforcing the affinity of *trans*-caryophyllene for lipophilic regions of the enzyme.

The calculated binding affinity for the *trans*-caryophyllene–1LML complex was $\Delta G_{\text{bind}} = -5.7$ kcal/mol, suggesting an energetically favorable interaction. Considering that *trans*-caryophyllene is a nonpolar and sesquiterpene molecule, its anchoring mechanism to the enzymatic target appears to be mediated mainly by hydrophobic interactions. The presence of conserved residues involved in the interactions, such as ARG and GLN, reinforces the relevance of the interacting site in the enzymatic activity, indicating a potential inhibitory effect of the ligand on the catalytic function of leishmanolysin.

2.7 | In Vitro Cytotoxic Activity

EOJ demonstrated moderate cytotoxic activity against HCT-116 (colon) and PC-3 (prostate) cancer cell lines, with IC₅₀ values ranging from 27.8 to 29.2 μg/mL (Table 6). These values fall below the 30 μg/mL threshold commonly used to define relevant cytotoxic potential. The activity is likely attributable to the synergistic effects of the oil's constituents, particularly γ -cadinene and *trans*-caryophyllene.

2.8 | Molecular Docking Studies Against Tumor Targets

Molecular docking analysis revealed detailed interactions between the main EOJ compounds— γ -cadinene and *trans*-caryophyllene—and key proteins associated with tumor progression. Notably, γ -cadinene displayed a binding free energy of -7.3 kcal/mol with the Nectin-4 protein (PDB ID: 4MAN), while *trans*-caryophyllene displayed layers similar to the human androgen receptor (AR, PDB ID: 1E3G).

Nectin-4 is a cell adhesion molecule frequently overexpressed in several types of cancer, including colorectal cancer. Its overexpression is associated with the promotion of tumor angiogenesis, cell signaling, and epithelial-mesenchymal transition (EMT), processes critical for tumor progression and metastasis. The interaction of γ -cadinene with Nectin-4 may interfere with these processes, contributing to the cytotoxicity observed in HCT-116 cells [46].

The AR, represented by the 1E3G structure, plays a central role in the survival and correction of prostate cancer cells, such as PC-3 (PDB: 1E3G) [47]. The binding of *trans*-caryophyllene to AR may inhibit its transcriptional activity, leading to the suppression of growth-promoting genes and inducing apoptosis in tumor cells.

These interactions involve critical hydrophobic materials, such as MET, LEU, and PHE, in the active regions of the proteins, indicating that γ -cadinene and *trans*-caryophyllene may act as natural inhibitors of these molecular targets. On the other hand, tridecanone exhibits lower binding free energy, establishing a secondary role in the cytotoxic activity of EOJ.

Taken together, these findings support the hypothesis that sesquiterpenes present in EOJ, particularly γ -cadinene and *trans*-caryophyllene, are key mediators of the cytotoxic effects observed in vitro in HCT-116 and PC-3 cell lines. The ability of these compounds to interact with critical proteins involved in tumor progression highlights their potential as candidates for the development of novel natural product-based anticancer therapies.

The interaction between the compound γ -cadinene and the protein Nectin-4 (PDB ID: 4MAN), represented in Figure 5, revealed a binding free energy (Table 7) (ΔG_{bind}) of -7.3 kcal.mol⁻¹, indicating a moderate to strong affinity. The analysis of the physical and chemical interactions in the active site showed a predominance of hydrophobic interactions, especially of the van der Waals, alkyl, and π -alkyl types. These interactions are essential for the stabilization of the protein-ligand complex, particularly when the ligand has a lipophilic structure, as is the case with γ -cadinene.

The hydrophobic residues identified in the interaction include ALA A:146, MET A:112, LEU A:134, and VAL A:130, which participated in alkyl contacts with the ligand side chains. These interactions promote the stable anchoring of the compound in the cavity of the protein active site. Furthermore, aromatic residues such as TYR A:105 and PHE A:101 established π -alkyl interactions with the carbocyclic ring of γ -cadinene. Such interactions are more direct and contribute significantly to the

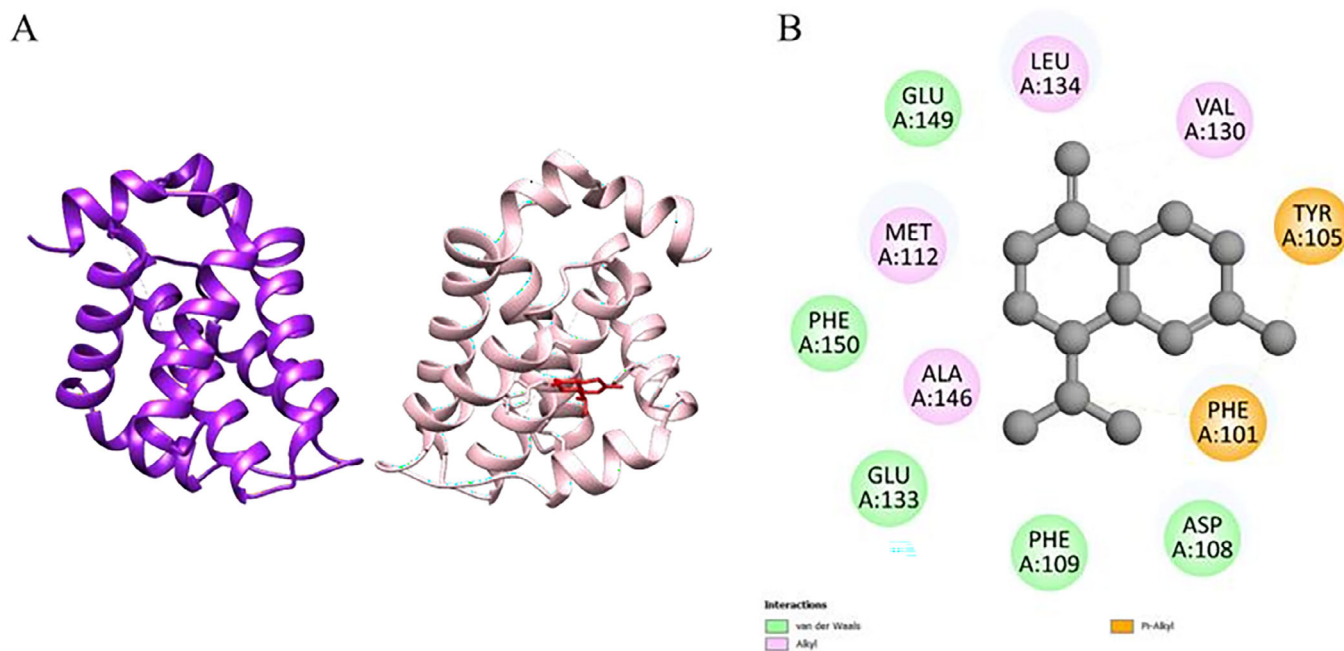


FIGURE 5 | 3D molecular docking of the ligand-protein complex with 4MAN (chain A color: pink; Chain B: purple) and γ -cadinene (color: red), illustrating the active binding site (A) with the respective interactions (B).

stability of the complex due to the complementarity between hydrophobic surfaces.

In addition, van der Waals interactions were observed with residues such as GLU A:133, GLU A:149, PHE A:109, and PHE A:150. Although these are weak forces individually, the cumulative effect of these non-covalent interactions promotes effective retention of the ligand in the active site. The absence of electrostatic interactions and hydrogen bonds reinforces that the observed affinity is attributed mainly to the lipophilic nature and hydrophobic interactions.

Figure 6 shows the interaction between the compound *trans*-caryophyllene and the human AR protein (PDB ID: 1E3G), associated with prostate cancer. The complex formed has a binding free energy (ΔG_{bind}) of $-7.3 \text{ kcal.mol}^{-1}$, a value that indicates high affinity between the ligand and the active site of the protein, favoring the hypothesis of potential inhibitory activity of *trans*-caryophyllene on this molecular target (Table 7).

The interactions observed in the active site of the protein are mostly hydrophobic, which agrees with the nonpolar nature of the compound. Among these interactions, the alkyl interactions with residues MET A:745, LEU A:704, VAL A:746, MET A:742, and LEU A:707 stand out. These hydrophobic contacts favor the accommodation of the ligand in the active cavity through shape complementarity and lipophilic surface.

Furthermore, the ligand establishes van der Waals interactions with a series of residues such as MET A:895, MET A:787, MET A:780, MET A:749, GLY A:708, LEU A:701, LEU A:873, ASN A:705, TRP A:741, THR A:877, and LEU A:880. These non-covalent interactions, although weak individually, act synergistically to stabilize the orientation of *trans*-caryophyllene in

the active site, contributing significantly to the total binding energy.

A π -alkyl interaction was also observed with the PHE A:764 residue, indicating a direct interaction between the unsaturated system of *trans*-caryophyllene and the aromatic ring of the amino acid. This type of interaction is important for the stable positioning of the ligand, in addition to reinforcing its affinity for the protein.

2.9 | Predicted ADMETox Profile (pkCSM)

In silico pharmacokinetic and toxicity predictions indicated that all three major compounds exhibited high intestinal absorption (>88%), wide tissue distribution ($VD_{ss} > 0.5 \text{ log L/kg}$), and good CNS permeability (for γ -cadinene and *trans*-caryophyllene). Despite their low water solubility, this can be addressed through appropriate formulation strategies.

Regarding metabolism, γ -cadinene was identified as a CYP3A4 substrate and CYP1A2 inhibitor, while *trans*-caryophyllene inhibited CYP2C19. None of the compounds were genotoxic in the Ames test or significant hERG channel inhibitors. Despite the promising pharmacological activities observed, the absorption, distribution, metabolism, excretion, and toxicity (ADMET) predictions indicate potential hepatotoxicity for γ -cadinene and tridecanone, raising concerns about their long-term safety profile, particularly under systemic administration.

However, *in silico* hepatotoxicity predictions are often based on structural alerts that do not always manifest *in vivo*, especially when metabolic biotransformation reduces compound reactivity. The γ -Cadinene, for instance, is a naturally occurring

TABLE 7 | Molecular affinity parameters of γ -cadinene, *trans*-caryophyllene, and tridecanone with 1E3G—Androgen receptor (tumor target), 1E31—Androgen receptor ligand-binding domain (apoptosis inhibitor), 1HVY—Human thymidylate synthase, 1K4T—Human DNA topoisomerase I, 1M17—Epidermal Growth Factor Receptor tyrosine kinase, 2ZCH -Crystal structure of human prostate specific antigen, 3OW3—Akt inhibitors, 4LXZ—Structure of Human HDAC2 (Hydrolase inhibitor), 4MAN—Apoptosis regulator Bcl-2, and 4OBE—GDP-bound Human Kras proteins.

Complex (Ligand-Protein)	$\Delta G_{\text{bind}}^{[a]}$ (kcal.mol⁻¹)	Amino acids that interact with ligand^[b]
γ -cadinene-1E3G	-6.9	LEU A: 704; ASN A: 705; MET A: 895; PHE A: 764; GLY A: 708; LEU A: 707; GLN A: 711; MET A: 745; ARG A: 752; META: 745; MET A: 787; MET A: 780; VAL A: 746; MET A: 749; LEU A: 873
γ -cadinene-1E31	-7.1	PHE A: 86; GLN A: 92; VAL A: 89; LYS A: 15; LEU A: 14; ASPA: 16; PHE A: 93; LEU A: 96; PHE A: 13; PHE A: 58; ARG A:18; LYS A: 91
γ -cadinene-1HVY	-6.7	LEU A: 187; PRO A: 188; ARG B: 176; ILE B: 177; ASP B: 174; VAL B: 164; THR B: 167; PRO A: 184; ILE B: 178; ARGB: 163; VAL B: 158; TRP A: 182; GLN B: 160
γ -cadinene-1K4T	-5.3	LYS A: 532; ALA A: 499; LYS A: 493; THR A: 501; THR A:498; SER A: 534; ASP A: 533; ARG A: 364
γ -cadinene-1M17	-7.1	ASP A: 831; VAL A: 702; MET A: 742; THR A: 766; LYS A: 721; ALA A: 719; LEU A: 820; GLY A: 772; MET A: 769; PHEA: 699; LEU A: 768; VAL A: 702; ASP A: 831
γ -cadinene-2ZCH	-6.5	HIS P: 57; SER P: 195; SER P: 214; ASP P: 102; TYR P: 94; LEU P: 95D; LEU P: 95I; GLN P: 174; GLY P: 216; TRP P:215; PHE P: 95H
γ -cadinene- 3OW3	-5.6	GLU A: 155; HIS A: 158; GLY A: 287; ASN A: 289; VAL A: 15; VAL A: 288; LYS A: 16; LEU A: 19; LYS A: 217; TRP A: 221; SER A: 159
γ -cadinene-4LXZ	-5.4	GLU A: 190; GLU A: 189; HIS A: 184; THR A: 213; TYR A:193; ASP A: 218
γ -cadinene- 4MAN	-7.3	MET A: 112; ALA A: 146; LEU A: 134; GLU A: 149; ASP A: 108; VAL A: 130; PHE A: 109; GLU A: 133; PHE A: 150; TYRA: 105; PHE A: 101
γ -cadinene-4OBE	-6.6	LYS A: 147; LEU A: 120; ASP A: 119; LYS A: 117; SER A: 145; ALA A: 146; PHE A: 28; ASN A: 116; ALA A: 18; GLY A:13; GLY A: 15; VAL A: 29; ASP A: 30
<i>trans</i> -caryophyllene- 1E3G	-7.3	MET A: 749; MET A: 745; VAL A: 746; LEU A: 707; PHE A: 764; MET A: 787; LEU A: 873; MET A: 742; MET A: 780; LEUA: 701; LEU A: 880; ASN A: 705; THR A: 877; MET A: 895; TRP A: 741; GLY A: 708; LEU A: 704
<i>trans</i> -caryophyllene-1E31	-6.6	ARG A: 18; LYS A: 15; GLU A: 40; GLN A: 92; LYS A: 91; VALA: 89; LEU A: 96; PHE A: 86; PHE A: 93; PHE A: 13; PHE A:58
<i>trans</i> -caryophyllene-1HVY	-5.2	THR B: 167; ASP B: 174; ASN B: 171; ARG B: 163; PRO A:188; PRO A: 193; LEU A: 187; TRP A: 182; ARG B: 176
<i>trans</i> -caryophyllene-1K4T	-5.6	LYS A: 443; THR A: 591; LYS A: 587; ARG A: 590; ALA A: 594; LEU A: 724; CYS A: 630; SER A: 719; HIS A: 632; ASNA: 722; THR A: 718; ARG A: 488
<i>trans</i> -caryophyllene-1M17	-6.9	LEU A: 694; LEU A: 768; ALA A: 719; THR A: 766; LYS A: 721; THR A: 830; ASP A: 831; LEU A: 820; VAL A: 702; GLYA: 772; MET A: 769
<i>trans</i> -caryophyllene-2ZCH	-6	GLU P: 218; GLY P: 216; TRP P: 215; HIS P: 57; LEU P: 95I; SER P: 214; PHE P: 95H; SER P: 192
<i>trans</i> -caryophyllene-3OW3	-5.6	LYS A: 16; LEU A: 19; VAL A: 15; SER A: 159; GLU A: 155; HIS A: 158; TRP A: 221; VAL A: 288; LYS A: 217; GLY A: 287
<i>trans</i> -caryophyllene-4LXZ	-5.6	THR A: 194; TYR A: 193; GLU A: 190; GLU A: 189; THR A:213; ASP A: 218
<i>trans</i> -caryophyllene-4MAN	-6.5	PHE A: 150; VAL A: 153; GLU A: 149; PHE A: 109; MET A: 112; PHE A: 101; ALA A: 146; ASP A: 108; VAL A: 130; LEUA: 134
<i>trans</i> -caryophyllene-4OBE	-5.7	ASP A: 30; ALA A: 18; PHE A: 28; GLU A: 31; VAL A: 29; TYRA: 32; GLY A: 15; SER A: 17; PRO A: 34; GLY A: 13; LYS A:117
tridecanone-1E3G	-5.3	VAL A: 746; MET A: 787; MET A: 780; PHE A: 764; LEU A: 873; GLN A: 711; MET A: 745; ARG A: 752; MET A: 749; LEUA: 707; MET A: 742; GLY A: 708; LEU A: 704; TRP A: 741; MET A: 895; ASN A: 705; THE A: 877
tridecanone-1E31	-5.2	PHE A: 58; LYS A: 91; ARG A: 18; PHE A: 86; LYS A: 15; LEUA: 14; GLU A: 94; PHE A: 93; GLN A: 92; VAL A: 89; LEU A:96; LEU A: 104; PHE A: 13

(Continues)

TABLE 7 | (Continued)

Complex (Ligand-Protein)	$\Delta G_{\text{bind}}^{\text{[a]}}$ (kcal.mol ⁻¹)	Amino acids that interact with ligand ^[b]
tridecanone-1HVV	-4.7	ASP B: 174; THR B: 167; ILE B: 177; ILE B: 178; VAL B: 164; GLN B: 160; PRO A: 184; VAL B: 158; PRO A: 188; LEU A:187; ARG B: 163; TRP A: 182; ARG B: 176; PRO A: 193
tridecanone-1K4T	-4	ASP A: 533; LYS A: 532; THR A: 501; LYS A: 493; SER A: 534; ARG A: 364; THR A: 498; ALA A: 499; HIS A: 367; GLNA: 421; PHE A: 361
tridecanone-1M17	-5.1	LEU A: 694; GLY A: 772; LEU A: 820; LEU A: 768; LYS A: 721; ALA A: 719; MET A: 769; VAL A: 702; ASP A: 831; THRA: 830; GLU A: 738; CYS A: 751; THR A: 766; LEU A: 764; MET A: 742
tridecanone-2ZCH	-4.6	LEU P: 95I; TRP P: 215; GLY P: 216; SER P: 226; CYS P: 191; THR P: 190; ASP P: 194; THR P: 213; SER P: 195; SERP: 192; SER P: 214; PHE P: 95H; GLU P: 218
tridecanone-3OW3	-4.2	SER A: 159; LEU A: 19; GLY A: 287; VAL A: 288; GLU A: 155; PHE A: 154; LYS A: 217; HIS A: 158; TRP A: 221; GLY A: 282
tridecanone-4LXZ	-3.3	GLU A: 189; ASP A: 186; GLU A: 190; TYR A: 193; THR A:213; HIS A: 184; ASP A: 218
tridecanone-4MAN	-4.8	GLU A: 176; ARG A: 124; HIS A: 181; TRP A: 173; TYR A:177; PHE A: 127; ALA A: 128; GLU A: 132; VAL A: 131
tridecanone-4OBE	-4.9	ASP A: 30; VAL A: 29; SER A: 17; TYR A: 32; ALA A: 18; GLYA: 15; LYS A: 117; LEU A: 120; ASP A: 119; PHE A: 28; ALAA: 146; LYS A: 147; ASN A: 116; SER A: 145

^[a] Power bond in best conformation.

^[b] Obtained with the Discovery Studio 2021 Client program.

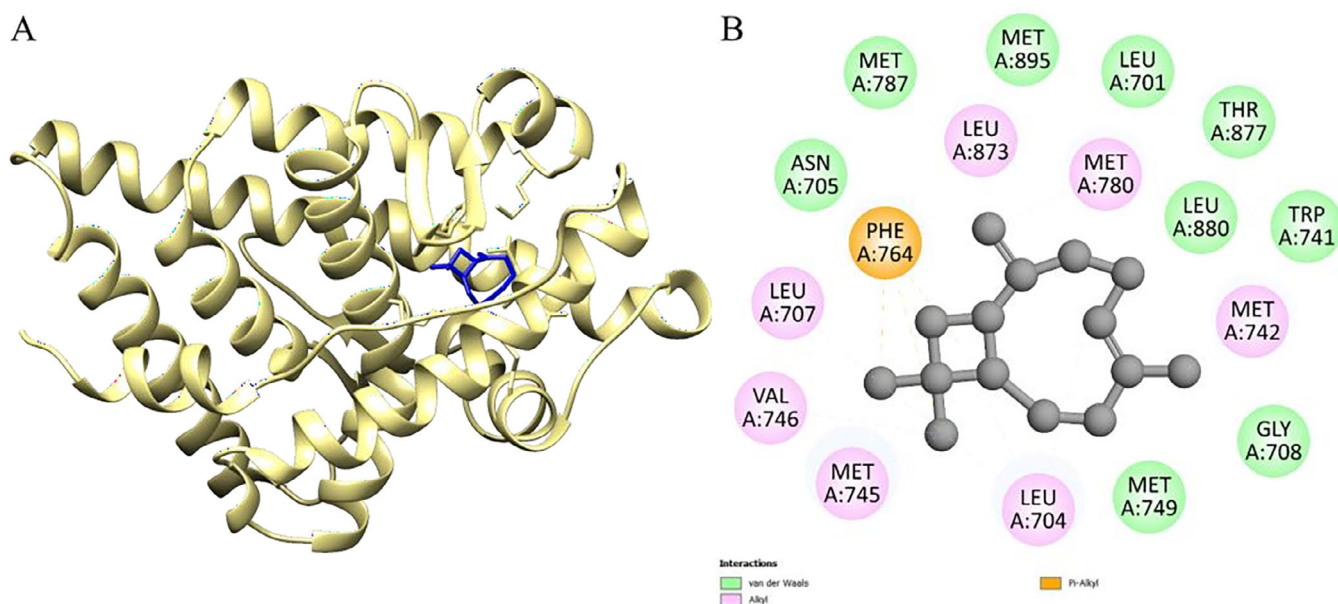


FIGURE 6 | 3D molecular docking of the ligand-protein complex with 1E3G (chain A color: khaki) and *trans*-caryophyllene (color: blue), illustrating the active binding site (A) with the respective interactions (B).

sesquiterpene found in low concentrations in edible spices and has not been definitively linked to liver toxicity in preclinical models. Formulation strategies such as nanoencapsulation or topical delivery may help mitigate systemic toxicity, as suggested in studies with *Zingiber officinale* and *Piper nigrum* essential oils [48]. Furthermore, the negative Ames test, high predicted absorption, and low hERG inhibition suggest that, with adequate pharmaceutical modulation, EOJ components retain viable therapeutic potential.

These results support the pharmacological viability of the major EOJ constituents, reinforcing the *in vitro* and *in silico* findings and highlighting their potential as drug candidates.

3 | Conclusions

In conclusion, EOJ exhibits promising biological potential. Steam distillation was used to isolate the EOJ, and GC-MS was used to

determine the composition of its chemicals. Chemical Statistical analysis revealed the presence of 24 compounds, with emphasis on γ -cadinene, *trans*-caryophyllene, and tridecanone as the major constituents. EOJ demonstrated antifungal activity against some *Candida* and *Cryptococcus* species, with IC₅₀ values ranging from 149 to 4790 $\mu\text{g}/\text{mL}$. EOJ inhibited the parasitic growth of *L. amazonensis* promastigotes and showed in vitro cytotoxic activity against HCT-116 and PC-3 cell lines, with similar IC₅₀ values for both oils. These results indicate that EOJ has significant potential as a source of active compounds with antifungal, antileishmanial, and cytotoxic effects. These findings highlight a promising therapeutic option for treating cancer and infectious forms of *Leishmania*, representing a promising research area for future therapeutic development.

4 | Experimental

4.1 | Plant Material

DL and FL of *P. microphyllus* were collected from the city of Parnaíba, Piauí, Brazil (02° 54' 17" S and 41° 46' 36" W). The species was identified by Dr. Ivanilza Moreira de Andrade from the Department of Biology, Federal University of Piauí, Brazil. A sample of the plant (TEPB voucher 27.152) was deposited at the Graziella Barroso Herbarium at the Federal University of Piauí (Teresina, PI, Brazil). This research was conducted under authorization of the Brazilian federal government (SISGEN registration no. AE263D6).

4.2 | Extraction and Analytical Chemistry

FL (6.4 kg) was washed with distilled water and steamed using an L20 D2 distiller to extract the EOJ. The same process was performed for DL, but the amount was lower (4.5 kg), and the oil yield was calculated according to the following formula: (weight of the EO obtained/weight of the plant material used) \times 100. GC-MS was used to analyze the EOJ. GCMS-QP2010 SE, AOC-5000 (Tokyo, Japan, Shimadzu) equipped with Rxi-5HT column (30 m \times 0.25 mm \times 0.25 μm) and stationary phase with 5% diphenyl dimethylpolysiloxane. An aliquot of 1 μL of sample solution was injected in the split mode (1:100), using helium as a drag gas in 1.02 mL.min⁻¹ flow, 220°C injection temperatures, source of ions at 250°C, and interface at 240°C. The GC-MS temperature was initially 60°C, increasing to 246°C at a 3 mL.min⁻¹ rate. The mass spectrometer with a quadruple analyzer was operated with electron impact ionization (EI) at 70 eV, detector at 290°C, solvent cut-off time of 3 min, and a mass scanning range of 47–500 Da.

The chemical identification of each oil substance was determined by its retention time and by comparison with data available in the Wiley Spectral Database. Retention indices (RIs) were calculated by co-injection with a homologous series of *n*-alkanes (C₈–C₂₀) under the same chromatographic conditions, according to the Van den Dool and Kratz method. Compound identification was based on comparison of RI values with literature data and by matching mass spectra with those from the Wiley library.

4.3 | Antibacterial Susceptibility Test

Antibacterial activity was evaluated using the broth microdilution method, as described by the M07-A10 protocol with modifications [49]. *Staphylococcus aureus* (ATCC 25923) and *Escherichia coli* (ATCC 25922) were the two strains of bacteria that were evaluated. Using 96-well microdilution plates, the MIC was determined by subjecting the strains to a series of two-fold dilutions of FL/DL-EOJ in triplicate. Their concentrations ranged from 92.9 to 4790 $\mu\text{g}/\text{mL}$. The plates were then incubated at 37°C for 24 h. Meropenem and Vancomycin were used as the positive controls for *E. coli* and *S. aureus*, respectively.

4.4 | Antifungal Susceptibility Test

Five distinct strains of yeast (*Candida parapsilosis* ATCC 22019, *Candida albicans* ATCC 10234, *Candida krusei* ATCC 6258, *Cryptococcus neoformans* ATCC 32269, and ATCC 24066) were tested to determine the antifungal activity of FL/DL-EOJ. All strains were provided by the Advanced Study Group in Medical Mycology (GEAMICOL) at the Federal University of Delta do Parnaíba. Amphotericin B (São Paulo, Brazil; Sigma-Aldrich) was used as the control. Strains of *Candida* spp. and *C. neoformans* were inoculated on Sabouraud Agar and incubated at 35°C for 24 and 48 h, respectively. The MIC was determined using 96-well plates and the broth microdilution method as outlined in the M27-A3 procedure [47]. The FL/DL-EOJ concentrations ranged from 92.9 to 4790 $\mu\text{g}/\text{mL}$ while the amphotericin B concentrations ranged from 0.03 to 16 $\mu\text{g}/\text{mL}$. The plates were then incubated at 35°C for 48 h. The MIC values were then determined visually and compared with the growth control. Each experiment was performed in triplicate.

4.5 | Investigation of Activity Against Promastigote Forms of *Leishmania amazonensis*

FL/DL-EOJ were diluted in 99% dimethyl sulfoxide (DMSO) (St. Louis, EUA, Sigma-Aldrich) at 80 mg/mL for the assays. *Leishmania amazonensis* strain (IFLA/BR/67/PH8) was obtained from the Center for Research in Medicinal Plants of the Federal University of Piauí. The parasites were grown in Schneider's Ten percent heat-inactivated fetal bovine serum (FBS) was added to the medium (St. Louis, EUA, Sigma-Aldrich), 100 U.mL⁻¹ penicillin (St. Louis, EUA, Sigma-Aldrich), and 100 $\mu\text{g}/\text{mL}$ Streptomycin (St. Louis, USA, Sigma-Aldrich) at 26°C. Promastigote forms of *L. amazonensis* in log phase growth (1×10^6 *Leishmania* 100 μL ⁻¹ of medium) were plated in a 96-well culture plate containing supplemented Schneider's (St. Louis, EUA, Sigma-Aldrich) medium. The concentration of the EOJ (6.25, 12.5, 25, 50, 100, 200, 400, and 800 $\mu\text{g}/\text{mL}$) was added and incubated for 48 h in a B.O.D. (biochemical oxygen demand) (Eletrolab EL202, São Paulo, Brazil) incubator at 26°C. Remaining 6 h to the end of this period, 20 μL of resazurin (1×10^{-3} mol.L⁻¹) was added. Afterward, the plate absorbance was read on a Biotek plate absorbance reader (model ELx800) at 550 nm. The results were expressed as the inhibition of parasite growth (%). Amphotericin B (90%) from Cristália (São Paulo, SP, Brazil) was used as a positive control at a concentration of 2 $\mu\text{g}/\text{mL}$. The negative control

was Schneider's (St. Louis, EUA, Sigma-Aldrich) containing promastigotes (1×10^6 cells/well). For parasites, cell viability was regarded as 100%. The blank was read for each concentration and control to avoid interference with the absorbance of the other medium compounds.

4.6 | In Vitro Cytotoxic Effect

The cytotoxicity of FL/DL-EOJ was tested against HCT-116 (colorectal carcinoma) and the human cancer cell line PC-3 (prostate adenocarcinoma). The cells were cultured and maintained in RPMI 1640 medium supplemented with 10% fetal bovine serum (St. Louis, USA, Sigma-Aldrich), 2 mM glutamine, 100 U/mL penicillin (St. Louis, USA, Sigma-Aldrich), and 100 μ g/mL streptomycin (St. Louis, USA, Sigma-Aldrich) at 37°C and 5% CO₂. In every experiment, 96-well plates containing 0.1×10^6 cells/mL for PC-3 and 0.7×10^5 cells/mL for HCT-116 were used for cell plating. After 24 h, FL/DL-EOJ samples (0.78–50 μ g/mL) dissolved in 1% DMSO (St. Louis, EUA, Sigma-Aldrich) were added to each well, and the cultures were incubated for 72 h. The control group received the same amount of DMSO (St. Louis, EUA, Sigma-Aldrich). The ability of living cells to convert 3-(4,5-dimethyl-2-thiazolyl)-2,5-diphenyl-2H-tetrazolium bromide (MTT), a yellow dye, into a purple formazan product was used to measure the development of tumor cells. Following the incubation period, the plates underwent centrifugation, and a new medium containing MTT (0.5 mg/mL) in 150 μ L was added. After three hours, the plates were centrifuged, 150 μ L DMSO was used to dissolve the MTT formazan product, and the absorbance at 595 nm was recorded. Doxorubicin (0.009–5 μ g/mL) was used as the positive control.

4.7 | Computational Studies ADME/Tox

Pharmacokinetic parameters related to the ADMET of the γ -cadinene, *trans*-caryophyllene, and tridecanone were provided with the online server pkCSM (<https://biosig.lab.uq.edu.au/pkcsml/>) [50], through the analysis of the monosaccharides of Cashew Gum SMILES file on the server, in which all the results obtained were considered for further discussion.

4.8 | In silico Protocol

Obtaining ligand structures and optimization. The 3D structure of γ -cadinene, *trans*-caryophyllene, and tridecanone was designed and optimized using GaussView 5 and Gaussian 09w software, respectively. The optimization was carried out employing the density functional theory method [51] with the hybrid B3LYP functional [52] and the STO-3 g basis set [53].

4.9 | For Fungal Proteins

For fungal activity, we selected lanosterol 14 α -demethylase (PDB ID: 6UEZ), a key enzyme in ergosterol biosynthesis and the primary target of azole antifungals, directly linked to fungal membrane integrity. The 3D structures of proteins were obtained from the online Protein Data Bank (PDB) server.

4.10 | For Leishmania Proteins

For *Leishmania*, docking was performed against leishmanolysin (gp63) (PDB ID: 1LML), which is a zinc-dependent metalloprotease abundantly expressed on the surface of *Leishmania* parasites, anchored by glycosylphosphatidylinositol (GPI). It plays a crucial role as a virulence factor by protecting promastigotes against complement-mediated lysis through the cleavage of C3b into iC3b, thereby facilitating parasite uptake by macrophages [54]. Moreover, gp63 contributes to host immune evasion by degrading cytokines and signaling molecules, modulating oxidative stress responses, and impairing macrophage microbicidal activity. These properties make leishmanolysin an essential determinant of parasite survival within host cells and a relevant molecular target for the development of anti-leishmanial therapeutics [54]. The 3D structures of proteins were obtained from the online PDB server, with the code 1LML. The Computed Atlas of Surface Topography of proteins (CASTp) 3.0 server was used to define the area, shape, volume, and likely region of the protein's active site.

4.11 | For Tumoral Proteins

The AR (1E3G) was included due to its central role in sustaining prostate cancer cells such as PC-3. Survivin (1E31) is an inhibitor of apoptosis highly expressed in tumors and associated with chemoresistance. Thymidylate synthase (1HVY) is essential for DNA synthesis and represents a classical target of antimetabolite drugs. DNA topoisomerase I (1K4T) regulates DNA topology and is critical for replication. The epidermal growth factor receptor (1M17) mediates proliferative signaling in solid tumors. The prostate-specific antigen (2ZCH) acts as a biomarker and effector in prostate cancer. Akt kinase (3OW3) is a central regulator of the PI3K/Akt/mTOR pathway, frequently hyperactivated in malignancies. Histone deacetylase 2 (4LXZ) modulates chromatin remodeling and gene expression, being linked to tumor progression. The anti-apoptotic protein Bcl-2 (4MAN), targeted by navitoclax analogs, plays a pivotal role in cell survival. Finally, GDP-bound KRas (4OBE) represents the inactive form of a critical GTPase frequently mutated in human cancers. Together, these targets encompass multiple molecular pathways, enabling a comprehensive evaluation of the antitumor potential of the essential oil constituents. The protein targets were retrieved from the RCSB PDB (IDs: 1E3G, 1E31, 1HVY, 1K4T, 1M17, 2ZCH, 3OW3, 4LXZ, 4MAN, and 4OBE). Water molecules and irrelevant ligands were removed using UCSF Chimera. Active sites were predicted using PrankWeb. Ligand and protein preparations were performed using AutoDockTools, which added polar hydrogens and Gasteiger charges.

4.12 | Molecular Docking

All docking procedures and the preparation of ligands and proteins were conducted using AutoDockTools 1.5.6, and the docking simulations were performed with AutoDock Vina [58]. Gasteiger partial charges were calculated after the addition of hydrogen [55]. Nonpolar hydrogen atoms of the protein and ligand were subsequently merged. A cubic box of $30 \times 30 \times 30$ points was generated for the whole protein target. For a more

detailed analysis, the coordinates of the selected complexes were chosen by the criterion of the lowest docking conformation of the cluster with the lowest energy in combination with a visual inspection [56–58]. The best binding poses were visualized with BIOVIA Discovery Studio and UCSF Chimera.

4.13 | Statistical Analysis

Raw absorbance data (resazurin and MTT assays) were blank-corrected. For each assay, results were expressed relative to the vehicle control (1% DMSO). No data transformation was applied. Outliers were not removed; when technical failures were suspected, the experiment was repeated. Data are presented as mean \pm SD. Unless otherwise stated, experiments were performed in three independent runs ($n = 3$), with technical replicates as described in the corresponding methods/legends. For antileishmanial assays, differences versus the negative control were assessed by one-way analysis of variance (ANOVA) followed by Dunnett's multiple-comparisons test. For ANOVA-based analyses, assumptions of normality and homoscedasticity were not formally tested due to the small sample size; data were inspected for gross deviations. Concentration–response curves were fitted by nonlinear regression to estimate IC₅₀ values with 95% confidence intervals (CIs 95%). All tests were two-tailed where applicable, with $\alpha = 0.05$. Analyses were performed using GraphPad Prism (version 6.0).

Acknowledgments

The authors thank Phytobios Company and the Biodiversity and Biotechnology Research Center (BIOTEC) for providing technical support.

Author Contributions

Juniel Cruz Silva: conceptualization, data curation, formal analysis, funding acquisition, and investigation. **Maria Gabriela Araújo Mendes:** investigation. **Paulo Sérgio de Araujo Sousa:** investigation, writing – original draft, and writing – review and editing. **Alyne Rodrigues de Araújo:** investigation, validation, and visualization. **Michel Muálem de Moraes Alves:** investigation. **Fernando Aécio de Amorim Carvalho:** investigation, validation, and visualization. **Tatiane Caroline Daboit:** investigation, validation, and visualization. **José de Sousa Lima Neto:** investigation. **Ygor Victor Ferreira Pinheiro:** investigation, validation, and visualization. **Ytallo da Costa Sousa:** investigation, validation, and visualization. **Edymilaís da Silva Sousa:** investigation. **José Delano Barreto Marinho Filho:** investigation. **Ana Jérsia Araújo:** investigation, validation, and visualization. **Sidney Gonçalves de Lima:** investigation, validation, and visualization. **Leiz Maria Costa Vêras:** formal analysis, funding acquisition, investigation, resources, visualization, writing the original draft, and writing – review and editing.

Conflicts of Interest

The authors declare no conflicts of interest.

Funding

The authors received no specific funding for this work.

Data Availability Statement

The authors have nothing to report.

References

1. A. Kapourani, K. N. Kontogiannopoulos, and P. Barmapalexis, “A Review on the Role of Pilocarpine on the Management of Xerostomia and the Importance of the Topical Administration Systems Development,” *Pharmaceuticals* 15 (2022): 762, <https://doi.org/10.3390/ph15060762>.
2. P. Singh, T. Garasiya, V. Ajila, S. Sengupta, A. Datta, and M. Nivean, “Efficacy and Safety of Pilocarpine Hydrochloride Ophthalmic Solution USP 1.25% w/v Versus Placebo Ophthalmic Solution for the Treatment of Presbyopia—A Multicentric Clinical Trial,” *Indian Journal of Ophthalmology* 73 (2025): 1251, https://doi.org/10.4103/ijoo.IJO_1172_24.
3. L. M. Veras, M. A. Guimaraes, Y. D. Campelo, et al., “Activity of Epiisopiloturine against *Schistosoma mansoni*,” *Current Medicinal Chemistry* 19 (2012): 2051–2058, <https://doi.org/10.2174/092986712800167347>.
4. Y. D. M. Campelo, A. C. Mafud, L. M. C. Vêras, et al., “Synergistic Effects of *in Vitro* Combinations of Piplartine, Epiisopiloturine and Praziquantel Against *Schistosoma mansoni*,” *Biomedicine & Pharmacotherapy* 88 (2017): 488–499, <https://doi.org/10.1016/j.biopha.2017.01.033>.
5. A. C. J. Rodrigues, A. C. M. Carlotto, M. D. Gonçalves, et al., “Exploring the Leishmanicidal Potential of Terpenoids: A Comprehensive Review on Mechanisms of Cell Death,” *Frontiers in Cellular and Infection Microbiology* 13 (2023): 1185947, <https://doi.org/10.3389/fcimb.2023.1260448>.
6. A. G. Atanasov, S. B. Zotchev, V. M. Dirsch, et al., “Natural Products in Drug Discovery: Advances and Opportunities,” *Nature Reviews Drug Discovery* 20 (2021): 200–216, <https://doi.org/10.1038/s41573-020-00114-z>.
7. A. M. Malacrida and R. T. Zanardo, “Resistência Antimicrobiana e Novos Antibióticos: Desafios e Avanços na Luta contra Infecções,” *Nativa Rev Ciênc Soc Norte Mato Grosso* 3 (2025): 1.
8. J. V. S. Pereira, I. C. Guedes, M. H. S. Vieira, et al., “A Leishmaniose como Doença Negligenciada: Impactos Epidemiológicos, Sociais e Clínicos no Contexto Nordestino,” *Cad Pedagógico* 22 (2025): e18187, <https://doi.org/10.54033/cadpedv22n9-199>.
9. D. J. Newman and G. M. Cragg, “Natural Products as Sources of New Drugs Over the Nearly Four Decades From 01/1981 to 09/2019,” *Journal of Natural Products* 83 (2020): 770–803, <https://doi.org/10.1021/acs.jnatprod.9b01285>.
10. A. I. Hussain, F. Anwar, S. T. H. Sherazi, and R. Przybylski, “Changes in Basil (*Ocimum basilicum* L.) Essential Oil Composition Under Different Drying Methods,” *Food Chemistry* 108 (2008): 662, <https://doi.org/10.1016/j.foodchem.2007.11.033>.
11. M. Rahimmalek and S. A. H. Goli, “Evaluation of Six Drying Treatments With Respect to Essential Oil Yield, Composition and Color Characteristics of *Thymus daenensis* subsp. *Daenensis*. Celak Leaves,” *Industrial Crops and Products* 42 (2013): 613–619, <https://doi.org/10.1016/j.indcrop.2012.06.020>.
12. R. C. Silva, R. E. S. Diniz, V. G. Rodrigues, and S. R. Machado, “Leaf Anatomy and Essential Oil Composition of *Pilocarpus microphyllus* Stapf Ex Wardleworth (Rutaceae),” *Revista Brasileira de Farmacognosia* 17 (2007): 210, <https://doi.org/10.1590/S0102-695X2007000200016>.
13. J. G. Melo, U. P. Albuquerque, T. L. G. Lemos, et al., “Essential Oils From Leaves of *Pilocarpus spicatus* and *P. microphyllus*,” *Flavour and Fragrance Journal* 18 (2003): 247, <https://doi.org/10.1002/ffj.1191>.
14. T. L. G. Lemos, F. J. Q. Monte, M. C. Mattos, G. M. P. Santiago, and R. Braz-Filho, “Essential Oils From *Pilocarpus pennatifolius* and *Pilocarpus giganteus*,” *Journal of Natural Products* 53 (1990): 1430, <https://doi.org/10.1021/np50072a031>.
15. R. Guimarães, et al., “Influence of Drying on the Chemical Composition of Essential Oils: A Review,” *Industrial Crops and Products* 132 (2019): 401, <https://doi.org/10.1016/j.indcrop.2019.02.041>.
16. R. P. Adams, *Identification of Essential Oils by Ion Trap Mass Spectroscopy* (Academic Press, 2012).
17. R. P. Adams, *Identification of Essential Oil Components by Gas Chromatography/Mass Spectrometry* (Allured Publishing Corporation, 2007).

18. V. I. Babushok, P. J. Linstrom, and I. G. Zenkevich, "Retention Indices for Frequently Reported Compounds of Plant Essential Oils," *Journal of Physical and Chemical Reference Data* 40 (2011): 043101, <https://doi.org/10.1063/1.3653552>.
19. PHEROBASE. *The Kovats Retention Index: Isoledene (C15H24)*. Disponível em, <https://www.pherobase.com/database/kovats/kovats-detail-isoledene.php>.
20. C. H. V. Fidelis, P. T. B. Sampaio, P. M. Krainovic, F. Augusto, and L. E. S. Barata, "Correlation Between Maturity of Tree and GC × GC-qMS Chemical Profiles of Essential Oil From Leaves of *Aniba rosaedora* Ducke," *Microchemical Journal* 103 (2012): 76–80, <https://doi.org/10.1016/j.microc.2012.03.034>.
21. H. Kamli, A.-A. M. Ali, Y. H. Salem, A. Shaikh, and H. A. S. El-Nashar, "Chemical Profiling and Enzyme Inhibitory Activities of Essential Oil Isolated From Pistacia Khinjuk Leaves: Insights on GC-MS Analysis and Skin Aging-Relevant Enzymes," *Chemistry & Biodiversity* 21 (2024): e202302096, <https://doi.org/10.1002/cbdv.202302096>.
22. M. Z. Ozel, S. Yilmaz, and C. Ergin, "Analysis of Eucalyptus Camaldulensis Volatiles From Turkey Using DTD-GC-MS," *Journal of Essential Oil Bearing Plants* 13, no. 3 (2010): 297–312, <https://doi.org/10.1080/0972060X.2010.10643825>.
23. F. B. Holetz, G. L. Pessini, N. R. Sanches, D. A. G. Cortez, C. V. Nakamura, and B. P. Dias Filho, "Screening of Some Plants Used in the Brazilian Folk Medicine for the Treatment of Infectious Diseases," *Memorias Do Instituto Oswaldo Cruz* 97 (2002): 1027–1031, <https://doi.org/10.1590/S0074-02762002000700017>.
24. NCCLS, *Reference Method for Broth Dilution Antifungal Susceptibility Testing of Yeasts; Approved Standard—Second Edition*. NCCLS Document M27-A2 (2002).
25. A. B. Miller, R. G. Cates, M. Lawrence, et al., "The Antibacterial and Antifungal Activity of Essential Oils Extracted From Guatemalan Medicinal Plants," *Pharmaceutical Biology* 53 (2015): 548–554, <https://doi.org/10.3109/13880209.2014.932391>.
26. A. Nazzaro, F. Fratianni, L. De Martino, R. Coppola, and V. De Feo, "Effect of Essential Oils on Pathogenic Bacteria," *Pharmaceuticals* no. 6 (2013): 1451–1474, <https://doi.org/10.3390/ph6121451>.
27. F. Bakkali, S. Averbeck, D. Averbeck, and M. Idaomar, "Biological Effects of Essential Oils—A Review," *Food and Chemical Toxicology* 46 (2008): 446, <https://doi.org/10.1016/j.fct.2007.09.106>.
28. J. Tian, X. Ban, H. Zeng, J. He, Y. Chen, and Y. Wang, "The Mechanism of Antifungal Action of Essential Oil From Anethum Graveolens Seeds Against *Candida albicans*," *Journal of Medical Microbiology* 61 (2012): 1454, <https://doi.org/10.1099/jmm.0.045054-0>.
29. J. R. Perfect, "Cryptococcus Neoformans: The Yeast That Likes It Hot," *FEMS Yeast Research* 6 (2006): 463–468, <https://doi.org/10.1111/j.1567-1364.2006.00053.x>.
30. R. Rajasingham, R. M. Smith, B. J. Park, et al., "Global Burden of Disease of HIV-associated *Cryptococcal meningitis*: An Updated Analysis," *Lancet Infectious Diseases* 17 (2017): 873, [https://doi.org/10.1016/S1473-3099\(17\)30243-8](https://doi.org/10.1016/S1473-3099(17)30243-8).
31. M. das Graças Freire de Medeiros, A. C. da Silva, A. M. das Graças Lopes Citó, et al., "In Vitro Antileishmanial Activity and Cytotoxicity of Essential Oil From *Lippia sidoides* Cham," *Parasitology International* 60, no. 3 (2011), <https://doi.org/10.1016/j.parint.2011.03.004>. v. n.
32. T. Ueda-Nakamura, R. R. Mendonça-Filho, J. A. Morgado-Díaz, et al., "Antileishmanial Activity of Eugenol-rich Essential Oil From *Ocimum gratissimum*," *Parasitology International* 55 (2006): 99–105, <https://doi.org/10.1016/j.parint.2005.10.006>.
33. E. V. M. Costa, L. R. A. Rocha, S. L. A. Baliza, et al., "Antitumor Properties of the Leaf Essential Oil of *Zornia brasiliensis*," *Planta Medica* 81 (2015): 563, <https://doi.org/10.1055/s-0035-1545842>.
34. F. T. Silveira, R. Lainson, and C. E. P. Corbett, "Clinical and Immunopathological Spectrum of American Cutaneous Leishmaniasis With Special Reference to the Disease in Amazonian Brazil: A Review," *Instituto Oswaldo Cruz* 99 (2004): 239–251, <https://doi.org/10.1590/S0074-02762004000300001>.
35. E. Torres-Guerrero, M. R. Quintanilla-Cedillo, J. Ruiz-Esmenjaud, and R. Arenas, "Leishmaniasis: A Review," *Fl1000Research* 6 (2017): 750, <https://doi.org/10.12688/fl1000research.11120.1>.
36. J. S. Raut and S. M. Karuppaiyl, "A Status Review on the Medicinal Properties of Essential Oils," *Industrial Crops and Products* 62 (2014): 250–264, <https://doi.org/10.1016/j.indcrop.2014.08.013>.
37. I. V. Ogungbe and W. N. Setzer, "In-silico Leishmania Target Selectivity of Antiparasitic Terpenoids," *Molecules* 18 (2013): 7761–7847, <https://doi.org/10.3390/molecules18077761>.
38. J. Soto-Sánchez, "Could Natural Terpenes be an Alternative for the Treatment of Neglected Tropical Diseases?" *Chemical Biology and Drug Design* 103 (2024): e14470, <https://doi.org/10.1111/cbdd.14470>.
39. M. Mounira, *Essential Oils—recent Advances, New Perspectives and Applications* (IntechOpen, 2024), <https://doi.org/10.5772/intechopen.114379>.
40. G. M. Polanco-Hernández, A. Giménez-Turba, E. Salamanca, et al., "Leishmanicidal Activity and Immunomodulatory Effect of a Mixture of Lupenone and β -Caryophyllene Oxide," *Revista Brasileira de Farmacognosia* 31 (2021): 199–206, <https://doi.org/10.1007/s43450-021-00143-8>.
41. V. N. Holanda, T. G. S. Brito, J. R. S. Oliveira, et al., "Potential Effects of Essential Oil From *Plinia cauliflora* (Mart.) Kausel on Leishmania: In Vivo, in Vitro, and In Silico Approaches," *Microorganisms* 12 (2024): 207, <https://doi.org/10.3390/microorganisms12010207>.
42. D. Santos Porto, B. Da Costa Bernardo Port, J. Conte, et al., "Development of Ophthalmic Nanoemulsions of β -caryophyllene for the Treatment of *Acanthamoeba keratitis*," *International Journal of Pharmaceutics* 659 (2024): 124252, <https://doi.org/10.1016/j.ijpharm.2024.124252>.
43. P. B. Joshi, B. L. Kelly, S. Kamhawi, D. L. Sacks, and W. R. McMaster, "Targeted Gene Deletion of Leishmania Major Genes Encoding Developmental Stage-specific Leishmanolysin (gp63)," *Molecular Microbiology* 43 (2002): 751, <https://doi.org/10.1046/j.1365-2958.2002.02767.x>.
44. M. A. Gómez, I. Contreras, M. Halle, M. L. Tremblay, R. W. McMaster, and M. Olivier, "Leishmania gp63 Alters Host Signaling Through Cleavage-activated Protein Tyrosine Phosphatases," *Science Signaling* 2 (2009): ra58, <https://doi.org/10.1126/scisignal.2000213>.
45. M. M. Kulkarni, W. R. McMaster, E. Kamysz, W. Kamysz, D. M. Engman, and B. S. McGwire, "The Major Surface Metalloprotease of the Parasitic Protozoan Leishmania, gp63, Enhances Resistance to Antimicrobial Peptides," *Journal of Biological Chemistry* 283 (2008): 9369, <https://doi.org/10.1074/jbc.M709220200>.
46. Y. Liu, X. Han, L. Li, et al., "Role of Nectin-4 Protein in Cancer (Review)," *International Journal of Oncology* 59 (2021): 93, <https://doi.org/10.3892/ijo.2021.5220>.
47. P. M. Matias, P. Donner, R. Coelho, et al., "Structural Evidence for Ligand Specificity in the Binding Domain of the Human Androgen Receptor," *Journal of Biological Chemistry* 275 (2000): 26164–26171, <https://doi.org/10.1074/jbc.M004571200>.
48. A. Jacob, R. Nixon, D. Thirumurthy, S. Angel, and D. Halder, "Essential Oil Nano-Delivery Systems: Recent Developments and Emerging Applications," *Natural Product Communications* 20, no. 11 (2025), <https://doi.org/10.1177/1934578X251390689>.
49. CLSI. *Methods for Dilution Antimicrobial Susceptibility Tests for Bacteria That Grow Aerobically; Approved Standard—Ninth Edition*. CLSI Document M07-A9 (2012).
50. D. E. V. Pires, T. L. Blundell, and D. B. Ascher, "pkCSM: Predicting Small-Molecule Pharmacokinetic and Toxicity Properties Using Graph-Based Signatures," *Journal of Medicinal Chemistry* 58 (2015): 4066–4072, <https://doi.org/10.1021/acs.jmedchem.5b00104>.

51. R. E. Stratmann, J. C. Burant, G. E. Scuseria, and M. J. Frisch, "Improving Harmonic Vibrational Frequencies Calculations in Density Functional Theory," *Journal of Chemical Physics* 106, no. 24 (1997): 10175–10183, <https://doi.org/10.1063/1.473326>.
52. A. D. Becke, "Density-functional Thermochemistry. III. The Role of Exact Exchange," *Journal of Chemical Physics* 98 (1993): 5648–5652, <https://doi.org/10.1063/1.464913>.
53. J. B. Collins, P. R. von Schleyer, J. S. Binkley, and J. A. Pople, "Self-consistent Molecular Orbital Methods. XVII. Geometries and Binding Energies of Second-row Molecules. A Comparison of Three Basis Sets," *Journal of Chemical Physics* 64 (1976): 5142–5151, <https://doi.org/10.1063/1.432629>.
54. A. Chan, J. M. Ayala, F. Alvarez, et al., "The Role of *Leishmania* GP63 in the Modulation of Innate Inflammatory Response to *Leishmania Major* Infection," *PLoS ONE* 16 (2021): e0262158, <https://doi.org/10.1371/journal.pone.0262158>.
55. J. Gasteiger and M. Marsili, "Iterative Partial Equalization of Orbital Electronegativity — A Rapid Access to Atomic Charges," *Tetrahedron* 36 (1980): 3219–3228, [https://doi.org/10.1016/0040-4020\(80\)80168-2](https://doi.org/10.1016/0040-4020(80)80168-2).
56. V. C. De Sousa, R. De Cássia Viana Carvalho, K. G. Dos Reis Barcelar, et al., "Synthetic Hydrazones: *In Silico* Studies and *In Vitro* Evaluation of the *Antileishmania* Potential," *Toxicology in Vitro* 88 (2023): 105560, <https://doi.org/10.1016/j.tiv.2023.105560>.
57. N. Mulinari Turin De Oliveira, B. Barbosa Da Luz, V. S. Schneider, et al., "Dietary Polysaccharides From Guavira Pomace, a co-product From the Fruit Pulp Industry, Display Therapeutic Application in Gut Disorders," *Food Research International* 156 (2022): 111291, <https://doi.org/10.1016/j.foodres.2022.111291>.
58. J. A. Rocha, N. C. S. Rego, B. T. S. Carvalho, et al., "Computational Quantum Chemistry, Molecular Docking, and ADMET Predictions of Imidazole Alkaloids of *Pilocarpus microphyllus* With Schistosomicidal Properties," *PLoS ONE* 13 (2018): e0198476, <https://doi.org/10.1371/journal.pone.0198476>.